Journal of
Applied Remote Sensing

Global variability of midtropospheric carbon dioxide as measured by the Atmospheric Infrared Sounder

Thomas S. Pagano
Edward T. Olsen
Hai Nguyen
Alexander Ruzmaikin
Xun Jiang
Lori Perkins

SPIE

Global variability of midtropospheric carbon dioxide as measured by the Atmospheric Infrared Sounder

Thomas S. Pagano,[a,*] Edward T. Olsen,[a] Hai Nguyen,[a] Alexander Ruzmaikin,[a] Xun Jiang,[b] and Lori Perkins[c]

[a]California Institute of Technology, Jet Propulsion Laboratory, 4800 Oak Grove Drive, Pasadena, California, 91109

[b]University of Houston, Department of Earth and Atmospheric Sciences, 312 Science and Research 1, Houston, Texas, 77204

[c]NASA Goddard Space Flight Center, Science Visualization Studios, Greenbelt, Maryland, 20771

Abstract. The Atmospheric Infrared Sounder (AIRS) on the EOS Aqua spacecraft provides accurate and consistent measurements of midtropospheric carbon dioxide (CO_2) with global monthly coverage. The data are widely used for studies of vertical transport of CO_2 due to large-scale dynamics (e.g., ENSO, MJO, and the Walker Circulation). The purpose of this paper is to characterize the response of CO_2 in the midtroposphere, at the altitudes where AIRS is most sensitive, to geophysical changes at the surface across the globe. Our findings confirm that surface factors, as well as weather and climate patterns, impact the global variability of midtropospheric CO_2 as observed by AIRS. Despite a phase lag and a reduction in the seasonal amplitude observed in AIRS CO_2 relative to surface CO_2 measurements in the Northern Hemisphere, a significant correlation is observed between regional variability of CO_2 from AIRS and Moderate Resolution Imaging Spectroradiometer (MODIS)-derived Gross Primary Productivity at the surface, primarily in the high-latitude boreal forests during the peak of the growing season (July). A video of global AIRS CO_2 and MODIS vegetation index clearly shows the seasonal drawdown of CO_2 from the midtroposphere over highly vegetated areas in the northern latitudes. In the Southern Hemisphere, we see higher amplitude in the seasonal cycle, with the phase leading that of the surface. Both are indicative of interhemispheric transport. [DOI: 10.1117/1.JRS.8.084984]

Keywords: Atmospheric Infrared Sounder; carbon dioxide; midtroposphere; Moderate Resolution Imaging Spectroradiometer; seasonal cycle.

Paper 13531SSP received Dec. 19, 2013; revised manuscript received Apr. 17, 2014; accepted for publication Apr. 18, 2014; published online Jun. 16, 2014.

1 Introduction

Increases in atmospheric carbon dioxide (CO_2) over the last century due to anthropogenic sources have led to an increase in net radiative forcing, and net energy retained by the Earth.[1] The resulting warming is expected to increase the frequency and/or magnitude of severe weather events on global and regional scales. Surface measurements of atmospheric CO_2 have traditionally played an important role in improving our understanding of CO_2 global growth rates due to anthropogenic sources and potential impacts on the carbon cycle.[2] They provide a long-term record and represent the gold standard for accuracy and precision since surface measurements can be made in a controlled environment. While a large network of ground measurements exists today (e.g., the National Oceanic and Atmospheric Administration Earth System Research Laboratory (NOAA ESRL) global sampling network),[3] measurements on a global scale are limited for logistical reasons. Considering the potential costs to society of

*Address all correspondence to: Thomas S. Pagano, E-mail: tpagano@jpl.nasa.gov

0091-3286/2014/$25.00 © 2014 SPIE

increasing anthropogenic CO_2 emissions and current efforts to reduce emissions through regulation and incentives, a better understanding of the location of sources and sinks and their impact on the global flux is of extreme importance.

To fully understand global transport of CO_2, repeated measurements of its vertical and horizontal distribution are necessary. Relatively new measurement methodologies allow CO_2 concentrations to be measured higher in the atmosphere. The Total Carbon Column Observing Network (TCCON) is a network of stations using upward looking Fourier Transform Spectrometers (FTSs) to measure the solar absorption spectra in the near-infrared and provides total column CO_2 measurements.[4] The AirCore is an atmosphere sampling system that passively samples the atmosphere by relying on changes in ambient pressure and may be carried on balloons and aircraft as high as the stratosphere.[5] Vertical profiles reveal as much as a 5 ppm decrease in CO_2 from the bottom of the free troposphere to the midtroposphere (approximately 400 mb), depending on atmospheric conditions and locations.

Aircraft platforms enable high-spatial resolution measurements of the horizontal and vertical distribution of CO_2, as performed systematically by the Comprehensive Observation Network for TRace gases by AirLiners (CONTRAIL) program,[6] Civil Aircraft for the Regular Investigation of the atmosphere Based on an Instrument Container (CARIBIC) program,[7] and specialized campaigns including the High-performance Instrumented Airborne Platform for Environmental Research (HAIPER) pole-to-pole observations (HIPPO).[8] Both ground-based and aircraft-based systems provide excellent measurement accuracy; however, they lack the repeating global coverage required to track CO_2 changes resulting from global atmospheric circulation.

Satellite observations of CO_2 provide a long term, near-global-coverage data set, enabling studies of atmospheric circulation over multiple time scales and identification of large-scale sources and sinks. Current space-based systems employ two different passive techniques to estimate CO_2 abundances in the atmosphere: the first class includes instruments that use solar reflected energy to determine the total CO_2 column, such as SCIAMACHY,[9] GOSAT,[10] and the OCO-2[11] instrument to be launched in 2014. These instruments measure the total column CO_2 over the sunlit hemisphere. They have good surface sensitivity and work best when viewing land scenes or ocean scenes with sun glint. The second class of remote sensing instruments uses thermal infrared emission of the atmosphere to derive CO_2, and includes the AIRS on Aqua,[12] the Infrared Atmospheric Sounding Interferometer (IASI),[13] and the tropospheric emission spectrometer.[14] These instruments retrieve atmospheric CO_2 primarily in the midtroposphere with relatively low-spatial resolution, but with higher spatial and temporal coverage. A multiyear comparison of CO_2 from satellite data and ground-based FTSs (TCCON) finds that the AIRS CO_2 data provide superior coverage and accuracy over oceans as compared to SCIAMACHY V2.2 and GOSAT V01.xx, particularly over oceans.[15]

At first, the value of midtropospheric measurements was questioned due to the well-mixed nature of this gas and the small expected variability. However, midtropospheric AIRS CO_2 measurements are recognized as a consistent and stable tracer for detecting large-scale vertical transport in the midtroposphere.[16] The first meteorological processes studied using AIRS data were associated with tropical seasonal oscillations, [e.g., the Madden–Julian Oscillation (MJO)[17] and the El Niño Southern Oscillation (ENSO)[18,19]] and validation of atmospheric transport models including GEOS-Chem.[20] The simultaneity of AIRS CO_2 and AIRS O_3 soundings allows direct detection of polar stratospheric/tropospheric exchange and sudden stratospheric warming.[21] AIRS data have also been used to examine regional fluxes of CO_2 over land.[22,23] Recent studies by carbon flux inversion modelers show that the assimilation of AIRS CO_2 data should improve the accuracy of surface flux estimates, particularly when used in conjunction with OCO-2 or GOSAT.[24,25] The recent interest in using AIRS midtropospheric CO_2 data for surface flux inversion estimates inspires us to examine more closely the degree to which CO_2 in the midtroposphere responds to changes at the surface.

The response of midtropospheric CO_2 to changes at the surface is characterized by a phase and amplitude change in the (roughly sinusoidal) seasonal signal. Here, we compare the phase and amplitude of the AIRS midtropospheric CO_2 product to equivalent parameters from the NOAA Earth System Research Laboratory (ESRL, Boulder, Colorado) surface CO_2 database, and also to Gross Primary Productivity (GPP), which is an indicator for photosynthetic activity, derived from the Moderate Resolution Imaging Spectroradiometer (MODIS). The comparisons provide information on the transport time and degree of mixing between CO_2 at the surface and the region of the atmosphere where AIRS is most sensitive. A video of AIRS CO_2 concentrations and MODIS Enhanced Vegetation Index (EVI), used to derive GPP, was developed to clearly show the spatial correlation of the seasonal drawdown by the global boreal forests.

2 Atmospheric Infrared Sounder Instrument and Carbon Dioxide Data Product

AIRS is a hyperspectral infrared instrument on the EOS Aqua Spacecraft, launched on May 4, 2002. AIRS has 2378 infrared channels ranging from 3.7 to 15.4 μm, and a 13.5 km footprint at nadir. AIRS scans ± 49.5 deg from an orbit altitude of 705.3 km, covering 95% of the globe every day.[26] AIRS, in conjunction with the Advanced Microwave Sounding Unit (AMSU), produces temperature profiles with 1 K/km accuracy on a global scale, as well as water vapor profiles and trace gas amounts for CO_2, CO, SO_2, O_3, and CH_4. AIRS data are used for weather forecasting, climate process studies, and validating climate models. AIRS and the Aqua spacecraft are expected to continue operating beyond the year 2022.

Several international groups have successfully retrieved concentrations of midtropospheric CO_2 from AIRS using a variety of methodologies.[27] The CO_2 data discussed in this paper are produced by the NASA AIRS project and are available at the NASA GES/DISC. All AIRS data used in this paper are AIRS Science Team Version 5 products.[28] The AIRS CO_2 data are produced using the method of Vanishing Partial Derivatives (VPD).[29] The VPD method solves the CO_2 estimates by iteratively minimizing the root-mean square (RMS) difference between the observed cloud-cleared radiances and forward-calculated radiances for the AIRS retrieved atmospheric state in selected CO_2 channels using the AIRS radiative transfer algorithm. The VPD algorithm is based on the coordinate descent methodology, that is, it applies the minimization independently and sequentially to all geophysical parameters that impact the radiance of a given channel used to retrieve CO_2, e.g., atmospheric temperature, water vapor, ozone, and CO_2. The process is iterated until the radiance residuals are minimized or the change in CO_2 falls below 0.25 ppm. The resulting "Level 2" product yields over 15,000 midtropospheric CO_2 retrievals per 24-hour period, each with a horizontal footprint of 90×90 km. Extensive quality control is applied during the retrieval including: quality of the AIRS geophysical products, monotonically decreasing radiance residuals from one iteration to the next, and the constraint that the spatial homogeneity of a 2×2 set of retrievals (clusters) must be within 2 ppm in a RMS sense.

The vertical sensitivity of the AIRS CO_2 data product is a function of the channels used in the retrieval and the atmospheric state. Only one CO_2 value is provided for each retrieved footprint, and represents a weighted average value in the midtroposphere over the vertical profile defined by the averaging kernels. The averaging kernels (a measure of the vertical sensitivity to a change in a geophysical parameter) for the AIRS Version 5 CO_2 data product are shown in Fig. 1 for a variety of atmospheric conditions. Figure 1 indicates that the maximum sensitivity to CO_2 is profile dependent and generally lies in the midtroposphere between 300 and 500 mb.

The AIRS Level 2 CO_2 retrievals were compared[12] to aircraft measurements made in the midtroposphere by Machida et al.[30] The aircraft measurements were taken over the Pacific Ocean at $\geq$10 km altitude between Australia and Japan from September 2002 to March 2004. Comparisons of the individual AIRS CO_2 daily concentrations to the concentrations measured on the aircraft show an RMS deviation of less than 3.0 ppm with a bias of approximately 1.0 ppm (Matsueda-AIRS). Over a 14-month period, comparison of the AIRS monthly average CO_2 to the aircraft measurements indicates an RMS deviation of 1.2 ppm and a bias of 0.4 ppm.[29]

The AIRS Level 3 (L3) monthly gridded CO_2 data files are produced using a simple averaging of the valid Level 2 data points for the corresponding month in each $2.0° \times 2.5°$ (lat × lon) grid location. Considerably more samples are included in each bin of the monthly L3 data product, depending on location, hence we can expect improved precision as compared to the daily product. Independent comparisons of AIRS midtropospheric L3 CO_2 with CO_2 derived from ground-based FTS from TCCON sites show a bias of -1.8 ppm (FTS-AIRS) with a relative accuracy of better than 1 ppm.[15]

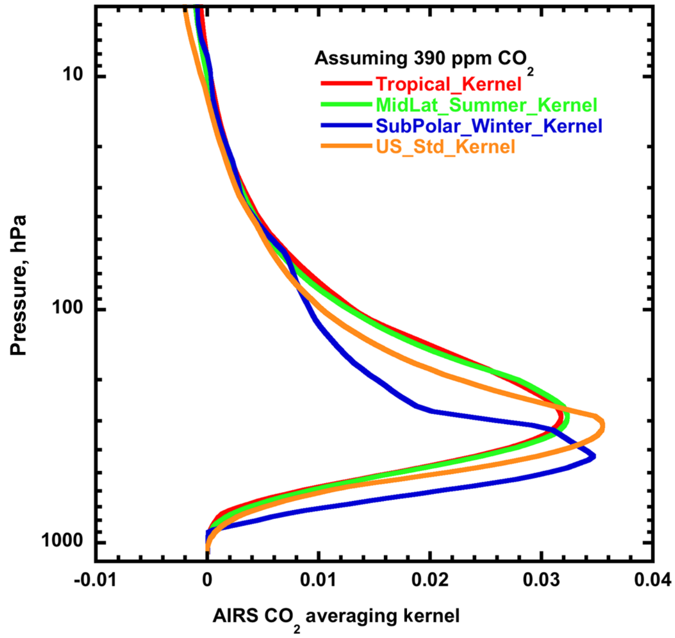

Fig. 1 AIRS Version 5 CO_2 averaging kernels. AIRS CO2 data are weighted in the midtroposphere region between 300 and 500 mb.

3 Comparison Data Sets

In order to examine the degree of coupling of CO_2 concentrations between the surface and the midtroposphere, we compare the AIRS data with CO_2 measurements made at the surface and with large-scale surface CO_2 sinks associated with global vegetation. For the AIRS data, we generate a provisional monthly climatology of AIRS midtropospheric CO_2, as well as zonal averages, from the AIRS Version 5 L3 CO_2 data set. We also create a set of provisional monthly climatologies for AIRS surface skin and 500 mb temperatures (from the AIRS L3 Standard Product), NOAA ESRL surface flask CO_2 measurements, and MODIS-derived GPP. The data sets used to derive the monthly climatologies are identified in Table 1 and discussed below.

3.1 *Atmospheric Infrared Sounder Carbon Dioxide Provisional Climatologies*

A provisional set of monthly climatologies of AIRS midtropospheric CO_2 concentrations was made from the AIRS Version 5 L3 data product to provide a measure of what AIRS would observe in any given month, and provides insight into the seasonal variability of this gas. In this section, we present the methodology used to create the climatologies and their zonal averages and, before comparing with other data sets, we provide an interpretation of the observed features in the data based on our current understanding and that of others cited in the literature.

Table 1 Data sets used in the comparison study and the source where the data files can be found.

Product	Instrument	Level	Source
Midtropospheric CO_2, $T_{500\ mb}$, T_{surf}	AIRS	L3	GES/DISC
Surface CO_2	*In-Situ*/flask	N/A	NOAA ESRL
EVI, T_{surf} (Used to derive GPP)	MODIS	L3	GES/DISC

3.1.1 *Constructing the Atmospheric Infrared Sounder carbon dioxide provisional climatologies*

The process for generating the mean CO_2 value in the AIRS climatologies first involves removing bad data points using the Level 3 AIRS CO2 data product quality control flags. The data are detrended to 2003 levels by removing a linear fit to the 8-year data set for each grid cell. The detrended monthly CO_2 mean values are averaged over all years for each month. Images of the resulting detrended mean CO_2 values are shown in Fig. 2 for all months. The 2003–2010 time frame was selected because it covers the period after which the AIRS instrument has stabilized

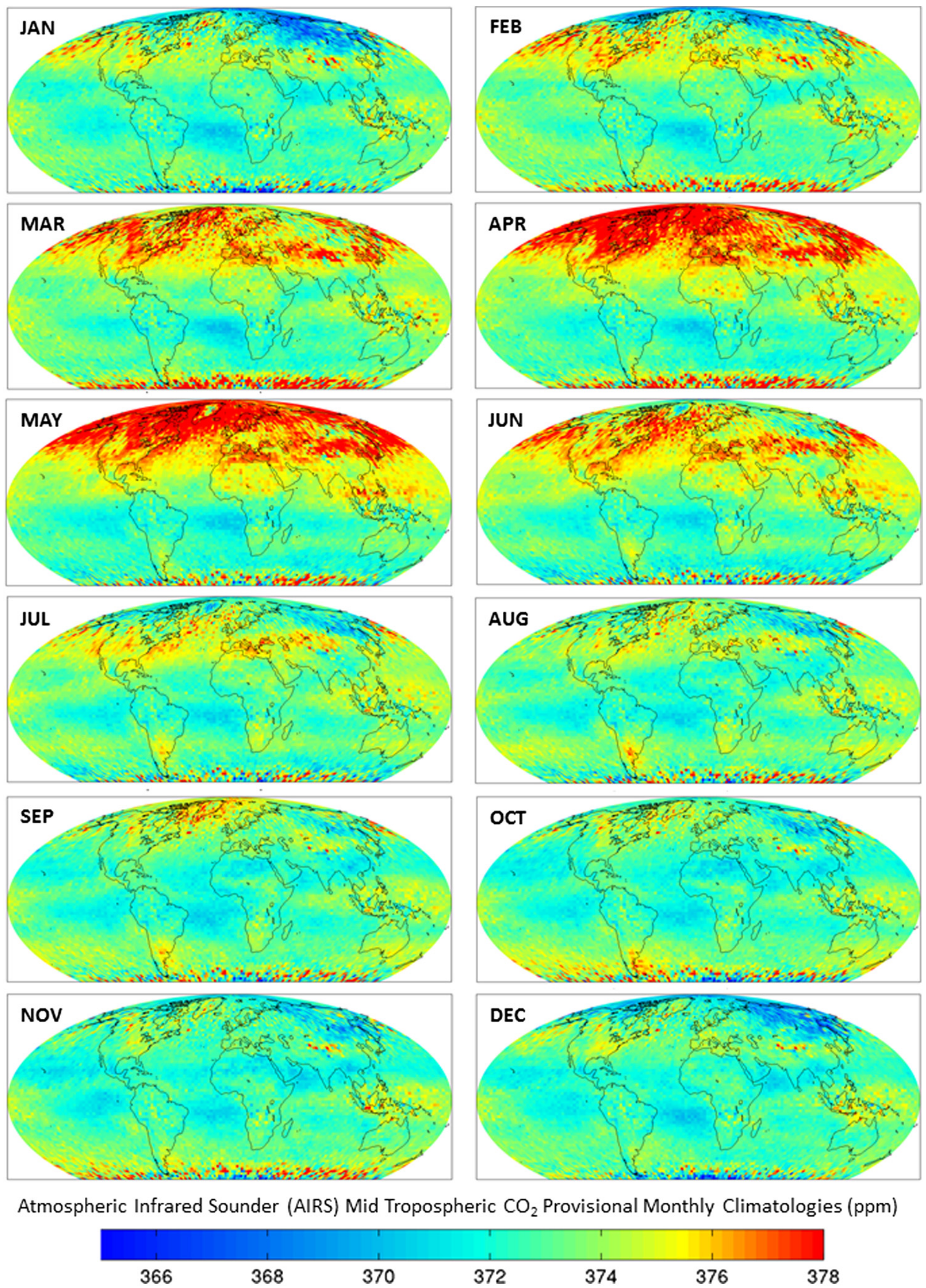

Fig. 2 Provisional monthly climatologies of AIRS midtropospheric CO_2 concentrations obtained from the AIRS Level 3 monthly data product over the years 2003–2010 (detrended to 2003 levels). AIRS high sensitivity enables identification of features related to global circulation patterns and surface sources and sinks.

and before the loss of AMSU channel 5. There is an AIRS-only retrieval that mitigates the loss of AMSU channel 5 and shows excellent consistency with the AIRS/AMSU retrieval, but at the time of this analysis, the data were not processed over the full mission time frame and showed no benefit over the AIRS/AMSU retrieval over the time frame selected. AIRS Version 6 CO_2 retrievals should be available in late 2014 or early 2015.

The climatologies reconstruct the original L3 monthly gridded CO_2 concentrations with a standard deviation of 1.48 ppm over the 1,092,793 L3 values used to construct the climatologies. 20,846 L3 CO_2 values were found to exceed the three-sigma threshold for an outlier percentage of 1.9%. This paper does not address trends in the AIRS CO_2 because the AIRS Version 5 temperature product showed a small but significant anomalous trend that could affect the CO_2 accuracy over a long time frame.[31]

The uncertainty of the AIRS CO_2 data for a given cell (latitude (i), longitude (j)), and month (m), σ_{ijm}, is calculated by combining the standard deviations in the L3 monthly gridded CO_2 data sets for that month over all years (k), σ_{ijkm}, according to

$$\sigma_{ijm} = \sqrt{\frac{\sum_{k=1}^{8} N_{ijkm}[D_{ijkm}^2 + \sigma_{ijkm}^2]}{\sum_{k=1}^{8} N_{ijkm}} - D_{ijm}^2}, \tag{1}$$

where

$$D_{ijm} = \frac{\sum_{k=1}^{8} N_{ijkm} D_{ijkm}}{\sum_{k=1}^{8} N_{ijkm}}, \tag{2}$$

and N_{ijkm} represents the number of L2 observations used to calculate the average CO_2 value, D_{ijkm}, in each grid cell of the L3 monthly data set. The uncertainty for the month of July is plotted in Fig. 3(a) and represents AIRS retrieval error and interannual variability of the scene. The higher uncertainty of the AIRS CO_2 measurements in the polar regions is driven by a lower yield and accuracy of the temperature profiles in these regions. Figure 3(b) shows the number of valid L2 retrievals used to make the mean for the July climatology. We see significantly fewer valid retrievals in the polar and tropical regions with high cloudiness (e.g., the ITCZ). Uncertainty remains low in the tropics despite the lower number of observations, most likely due to the higher accuracy of the temperature profiles in this region as compared to the polar regions.

3.1.2 *Zonal average Atmospheric Infrared Sounder carbon dioxide concentrations and uncertainty*

To improve the precision in the AIRS CO_2 data, we create zonal averages of the AIRS CO_2 monthly climatologies over 20° latitudinal bands. The zonal average seasonal dependence of the AIRS CO_2 data is shown in Fig. 4(a) for each zone, along with the seasonal dependence of other products as discussed below. The legend provides the center of each 20° zone (e.g., 0 represents $-10°$ to $+10°$). Features seen in the AIRS data are discussed in the next section.

We calculate the uncertainty in the zonal mean as the standard deviation of the mean values given in the climatologies for each zone. This method includes the precision of the measurements and retrievals as well as the natural variability within the zone. Figure 5 shows the anticipated uncertainty in the zonally averaged mean AIRS CO_2 concentrations using this method. We see a significant improvement compared to the gridded data, resulting in approximately 1 ppm uncertainty in the tropics and approximately 2–3 ppm uncertainty in the polar regions.

3.1.3 *Seasonal variability in the Atmospheric Infrared Sounder carbon dioxide data*

The seasonal variability in the AIRS CO_2 data is distinctive, yet subtle, in terms of absolute magnitude. Figure 6 shows the AIRS CO_2 zonal average means plotted as a function of zone for each of the 12 months. Zone spacing is 5° starting at 60°S since, at this time, data south of this latitude have not been released. Results for this region are available in Version 6 pending further validation.

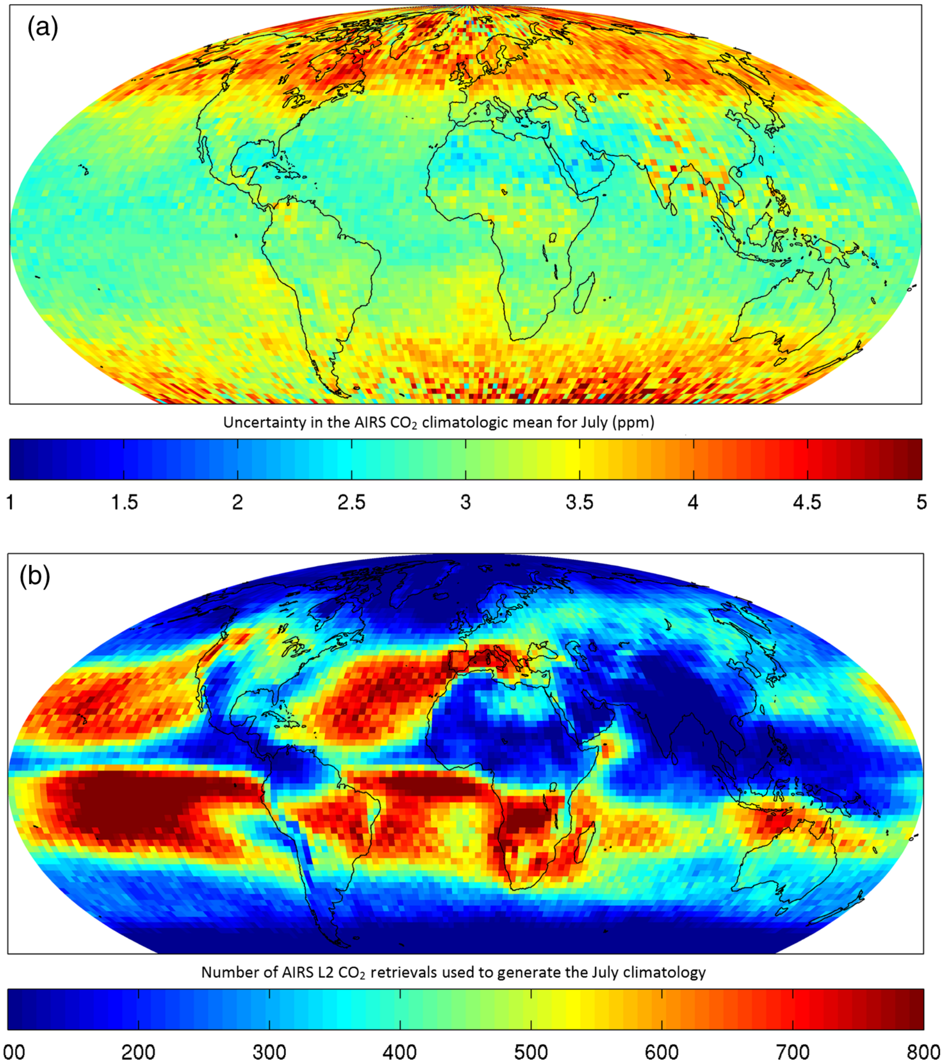

Fig. 3 (a) AIRS CO_2 data show higher uncertainties in the polar regions. (b) Uncertainty remains low in the tropics despite fewer observations in many areas due to clouds.

In the Southern Hemisphere (SH), we see lower seasonal variability with a seasonal cycle opposite that of the Northern Hemisphere (NH) at the same latitudes. This seasonal inversion has also been seen in the CONTRAIL data in the Western Pacific.[6] SH variability is primarily driven by interhemispherical transport.[32] In the SH tropics, we see a significant reduction in the seasonality of the zonal averages along with a curious depression of CO_2 values of about 1 ppm. We originally thought this was due to high-vegetation levels in this zone producing a drawdown in this region, but when we look at the AIRS CO_2 monthly climatologic means in Fig. 2, we see the depression to be located over the South Atlantic Ocean. Further exploration and model comparisons led to the discovery that this region experiences a large persistent downwelling of stratospheric air into the midtroposphere associated with a Walker cell, leading to lower CO_2 concentrations in this location.[33] The impact of the depression leads to an apparent "belt" of CO_2, poleward of the depression, alluded to in a prior work by these authors[27] and others using HIPPO observations.[8]

As we cross into the NH, we see a significant increase in the seasonality associated with the increase in deciduous forest and associated photosynthesis and respiration of CO_2. In the extratropics, near 40°N, we see a local increase in CO_2 associated with the major surface sources in this zone. Similar results are seen in the CONTRAIL data.[6] Poleward of 40°N, we see a significant increase in the amplitude of the seasonality with an apparent increase in the modes

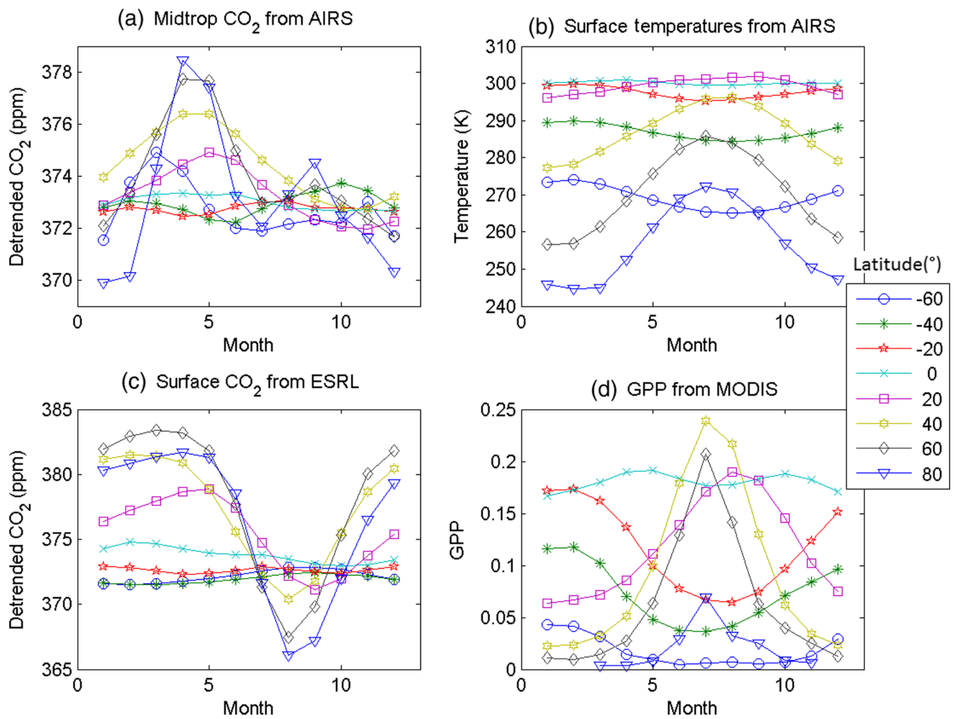

Fig. 4 Zonally averaged seasonal dependence between 2003 and 2010 for (a) AIRS MidTropospheric CO_2, (b) AIRS surface skin temperatures, (c) NOAA ESRL surface flask measurements, (d) MODIS-derived GPP.

of the oscillation (see also Fig. 4(a), zone at 80°). Higher concentrations in the Arctic in April and May could be related to CO_2 being transported north because of buildups of fossil fuels and biomass burning in winter in the south. The averaging kernel for AIRS in the polar regions peaks lower in altitude and could lead to an enhancement in the AIRS sensitivity. However, further validation of the AIRS data in this region is needed pending improved data sets for both AIRS (i.e., Version 6) and in-situ measurements in the midtroposphere in the polar regions.

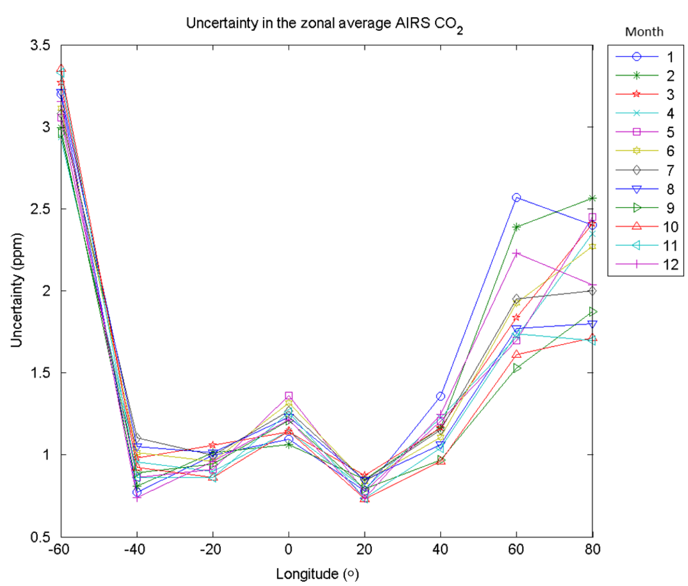

Fig. 5 Standard deviation of the zonally averaged AIRS CO_2 over 20° × 360° (Lat × Lon) zones from 60°S to 80°N. The uncertainty includes spatial and temporal variability within the zone as well as AIRS precision.

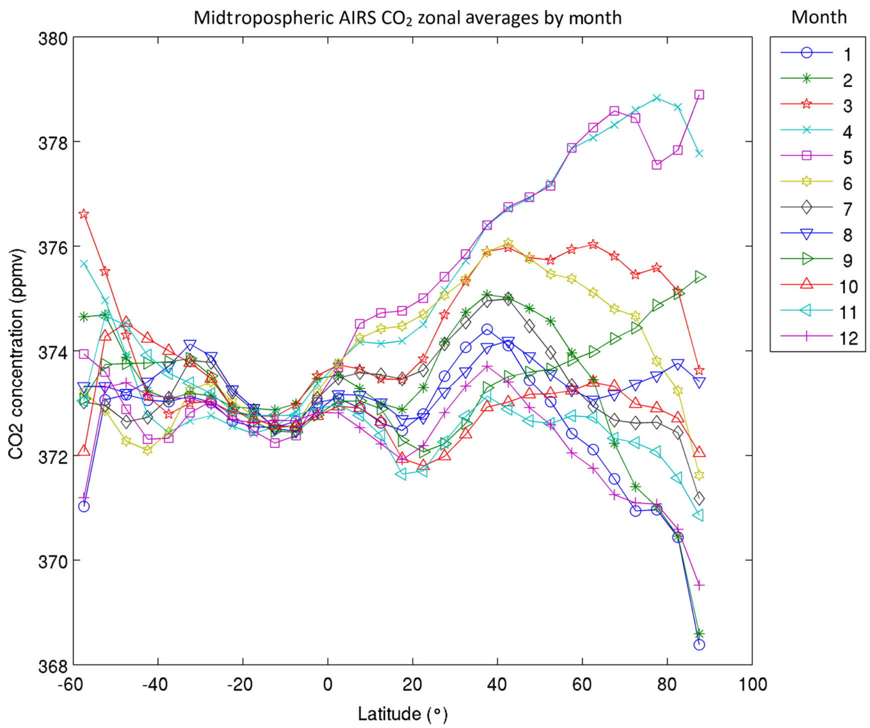

Fig. 6 AIRS midtropospheric CO_2 concentrations versus latitudinal zone for each month reveals global circulation patterns and the influence of surface sources and sinks.

3.2 *Atmospheric Infrared Sounder Midtropospheric and Surface Skin Temperatures*

We also examine AIRS midtropospheric and surface skin temperatures to explore potential correlations with CO_2 and GPP. Provisional monthly climatologies of AIRS 500 mb and surface skin temperature products were created by computing the average and standard deviation of ascending (daytime) and descending (nighttime) data from the AIRS Version 5 Standard Level 3 spatially gridded (1 deg ×1 deg) monthly data sets, for each month, over the time frame from 2003 to 2010, and by applying quality control contained within the L3 data set.[34] Zonal averages were calculated as for CO_2 and the resulting seasonal dependence of surface skin temperature is shown in Fig. 4(b) for each zone.

3.3 *Earth System Research Laboratory Surface Flask Measurements*

Comparing the seasonal signal of AIRS CO_2 to surface CO_2 data provides a direct measure of change in phase and amplitude from the surface to the midtroposphere due to atmospheric mixing and vertical transport. Additionally, since there are no sources or sinks of CO_2 in the free troposphere, we can consider it a tracer gas and use it to estimate the age of midtropospheric air on monthly timescales across the globe. Surface CO_2 data used in the analysis are obtained from the NOAA ESRL. The CO_2 mixing ratios reported in these data sets were measured by a nondispersive infrared absorption technique in air samples collected in glass flasks at NOAA ESRL carbon cycle cooperative global air sampling network sites.[35] Over 84 sites reported on a monthly basis are used in this analysis and their locations are shown in Fig. 7.

Monthly climatologic mean and uncertainty of the ESRL CO_2 were calculated by binning the valid data in 1 deg × 1 deg grid locations across the globe and computing statistics for each month over the time frame from 2003 to 2010. Zonal averages of the mean and uncertainty were then calculated as for CO_2 discussed above for all valid samples. The seasonal dependence of the ESRL CO_2 is shown in Fig. 4(c) for each zone.

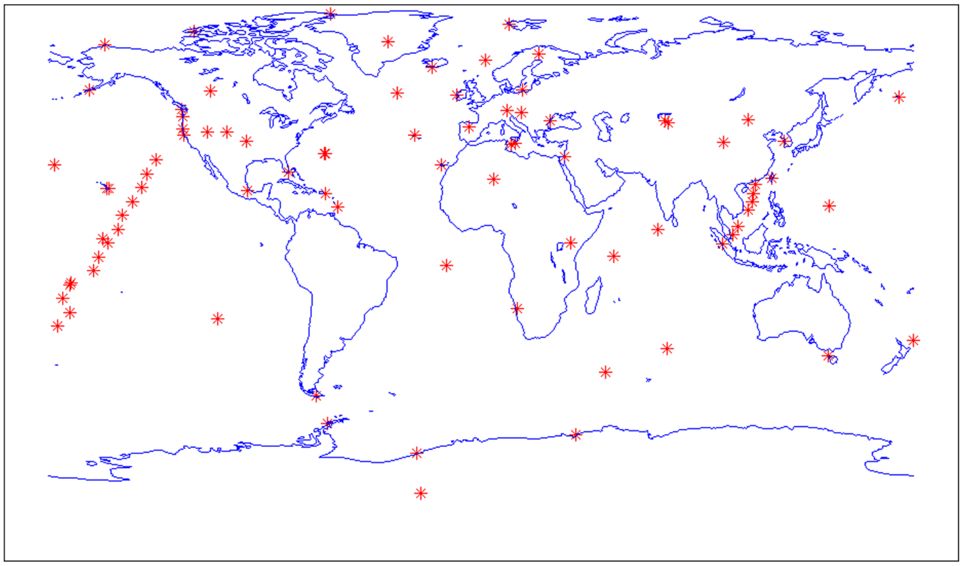

Fig. 7 Locations of ESRL CO_2 surface measurement sites used in the study.

3.4 *Moderate Resolution Imaging Spectroradiometer-Derived Gross Primary Productivity*

Terrestrial GPP is the largest global CO_2 flux, and along with respiration is one of the major processes controlling land atmosphere CO_2 exchange.[36] A set of monthly climatologies of GPP was developed from the MODIS data to examine the influence of large-scale surface sinks on midtropospheric CO_2 concentrations. The global nature of these satellite data sets provides a unique opportunity to analyze the regional correlation between the seasonal uptake of CO_2 and the annual increase in GPP. MODIS Level 3 GPP data were not available at the time of the analysis, hence a monthly GPP product was generated from monthly L3 gridded MODIS EVI[37] and nighttime land surface temperature (LST)[38] using a method outlined in Sims et al.[39] The process requires computation of the dimensionless quantities "scaled EVI," "scaled LST," and a slope term, m, that accounts for empirical correlations with the product of these variables and ground-based measurements of GPP such that

$$\mathrm{GPP} = (\text{scaled EVI} \times \text{scaled LST}) \times m. \tag{3}$$

The MODIS monthly L3 collection 5 EVI and LST data are gridded on 1 deg ×1 deg bins, and GPP was calculated for each bin. A map of the annual average GPP is shown in Fig. 8. Zonal mean and uncertainty of the resulting climatology were calculated as for the other products discussed above with the mean shown in Fig. 4(d).

4 Results

The collection of data used in this analysis has led to two significant observations. First, we see that CO_2 in the midtroposphere as measured by AIRS in the NH is more strongly coupled to the surface at the equator than it is at the poles. This result is based on our finding that the AIRS CO_2 seasonal cycle in the NH lags that of the surface by an amount that depends on latitude zone. We also see that midtropospheric CO_2 in the NH has less seasonal variability (captured in the amplitude) compared to that of the surface. Both effects become more pronounced as we go poleward from the equator as expected based on the higher convection in the tropics. Despite the damping relative to the surface in the NH, a significant correlation is observed in the regional variability of CO_2 in the midtroposphere and MODIS-derived GPP at the surface, primarily in the northern latitude boreal forests at the peak of the growing season (July). The second significant observation is that the amplitude and phase of the seasonal cycle of midtropospheric CO_2 in the SH are

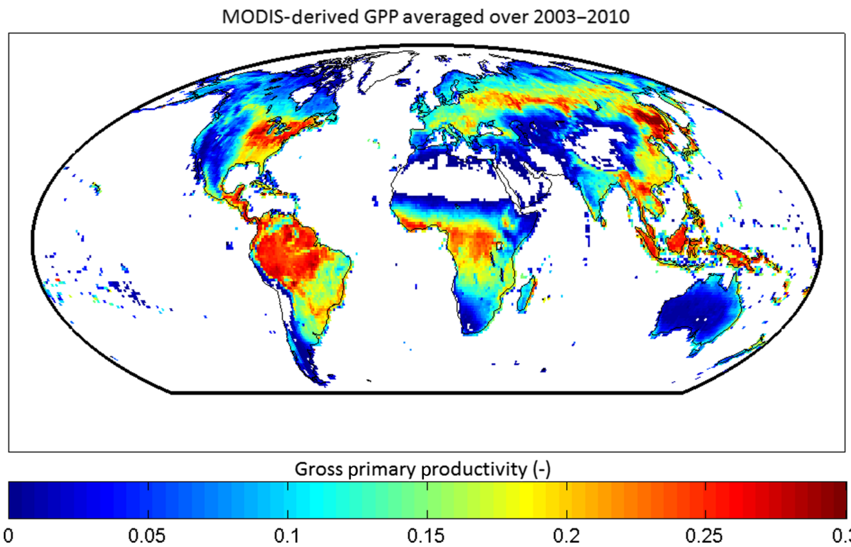

Fig. 8 MODIS-derived GPP used in the comparison, averaged over all months and years between 2003 and 2010.

higher and earlier than the surface, respectively, indicative of interhemispheric transport. These results can be used to validate vertical and interhemispheric transport mechanisms in atmospheric transport models.

4.1 *Zonal Phase and Amplitude of the Seasonal Cycle*

In this section, we present results comparing the phase and amplitude of the seasonal cycle in the zonal averages of AIRS midtropospheric CO_2 and temperature data, surface ESRL CO_2 data, and MODIS-derived GPP data.

The amplitude of the seasonal cycle is computed as the difference between the maximum and minimum of the zonal average monthly climatologic means for each product. Results are shown in Fig. 9(a) for CO_2, and Fig. 9(b) for temperature and GPP. All zones are 20 deg in latitude extent and average the full extent in longitude (180°W to 180°E) and the error bars represent the combined ± 1 sigma uncertainty of the maximum and minimum values used to calculate the amplitude. A distinct reduction in the amplitude of the seasonal cycle can be seen between the AIRS midtropospheric data and the NOAA ESRL surface data in the NH, as well as a consistent increase in seasonal amplitude poleward from the equator to 60°N. In the SH, we see a higher amplitude than the surface, most likely due to interhemispheric transport. Evidence of interhemispheric transport in the CO_2 seasonal cycle is also seen in the CONTRAIL data sets.[6] For reference, we also plot the amplitude variability for the temperature and GPP products in Fig. 9(b). Here, we see a reduction in the amplitude of midtropospheric temperatures relative to those at the surface as seen for CO_2. The GPP seasonal amplitude increases poleward except in the Arctic, most likely due to the transition from deciduous to evergreen forest in this region. The reduction in seasonal amplitude is not observed in the AIRS CO_2 in the Arctic and may indicate that GPP plays a lesser role in CO_2 concentrations than atmospheric circulation at these high latitudes.

Prior work by the authors has examined the trends, semiannual, and annual variability in the AIRS data using EOF analysis and attributes observed variability to atmospheric circulation patterns.[40] In a study using several atmospheric chemical transport models and surface flux estimates, a distinct semiannual oscillation appears in the predicted midtropospheric CO_2 concentrations[41] that can be attributed to the exchange of the surface with the biosphere. This latter work could explain the semiannual oscillations seen in the AIRS data using the EOF analysis, and indicate the presence of a distinct influence of the surface on the midtroposphere.

For comparison of the phase, we locate the time of the minimum in the seasonal cycle of zonally averaged CO_2 and time of the maximum for zonally averaged temperature and GPP.

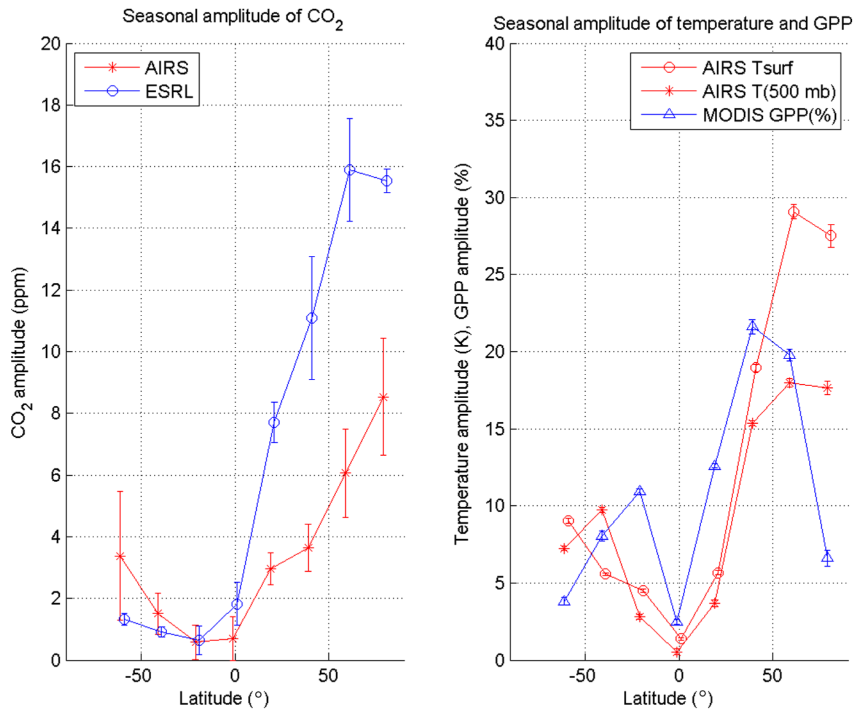

Fig. 9 Zonal average amplitude of the seasonal cycle for (a) AIRS and ESRL CO_2, and (b) AIRS Surface and Midtropospheric Temperatures (in K) and GPP (in %). Midtropospheric CO_2 seasonal cycle amplitudes are diminished in the NH due to mixing, but higher in the SH due to interhemispheric transport.

Results are shown in Fig. 10. The time of the minimum and maximum is found using cubic splines to improve temporal precision, and uncertainties in the time are found by applying the bootstrap method of varying the signal by a random fraction of the uncertainty.

Figure 10(a) shows a 1–4-month phase difference in the minimum of the seasonal cycle of CO_2 between the surface and midtroposphere depending on the zone with the most difference in the polar regions. The midtropospheric CO_2 lags the surface in the NH, most likely due to atmospheric mixing and circulation patterns and leads the surface in the SH, most likely due to interhemispheric transport. NH flights from the Philippines to China during the CARIBIC campaign show a minimum in CO_2 concentrations in September for the troposphere and in October for the lower stratosphere, about 1–2 months earlier than observed by AIRS.[7] The minimum of midtropospheric CO_2 at 40°S is seen between January and April in the CONTRAIL aircraft flights[6] as well as the bimodal seasonal cycle also seen in AIRS data shown in Fig. 4(a). GEOS-Chem model simulations agree with AIRS in the northern tropical latitudes but also lead the AIRS data by 1–2 months in the northern midlatitudes.[20] Differences are likely due to algorithm difficulties identifying the month of the minimum in the AIRS CO_2 and comparison data sets and differences in the vertical sensitivity of AIRS.

Figure 10(b) shows the month of maximum in the seasonal cycle of MODIS-derived GPP and AIRS temperatures. The month of maximum GPP correlates well with the month of minimum CO_2 at the surface, indicating GPP is a major player in the seasonal cycle of CO_2. The AIRS temperature and MODIS-derived GPP agree well, as expected, since warmer temperatures lead to higher GPP. We do not see a difference in the phase between the surface and midtropospheric temperatures as in CO_2, since CO_2 variability is primarily driven by surface phenomena and requires transport to the midtroposphere, while atmospheric temperature is driven by solar forcing and weather patterns. We observe no evidence of a correlation between the phase of the AIRS CO_2 and temperature products that would result from a retrieval error. The phase of GPP and temperature at the equator is ambiguous due to the weak and bi-modal seasonal cycle in this region and therefore is not included in the figure.

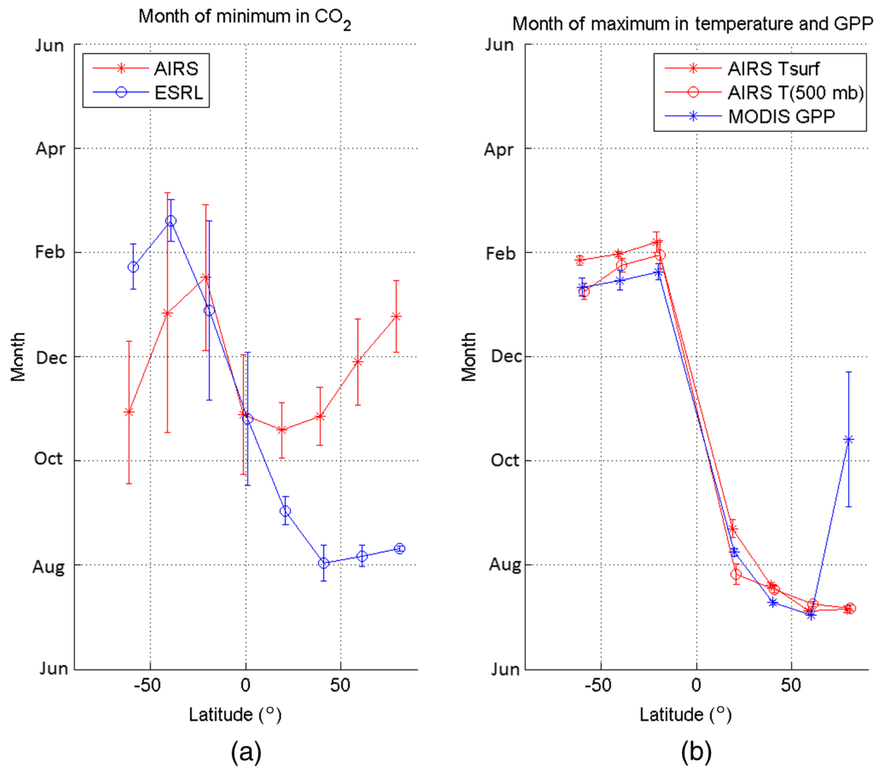

Fig. 10 (a) Minimum in the seasonal cycle of AIRS midtropospheric CO_2 lags that of the surface in the NH and leads in the SH. Differences are due to atmospheric circulation and interhemispheric transport. GPP highly influences the seasonal cycle of CO_2 at the surface as evidenced by high correlation of the month of minimum in CO_2 with the month of maximum MODIS-derived GPP and AIRS Temperature (b).

4.2 *Regional Correlation of Atmospheric Infrared Sounder Carbon Dioxide and Moderate Resolution Imaging Spectroradiometer-Derived Gross Primary Productivity*

The excellent spatial and temporal coverage of the AIRS and MODIS satellite data sets enable a unique study of the correlation of midtropospheric CO_2 with surface vegetation on a global scale. To examine the correlation, we create regional averages from the monthly climatologies of AIRS CO_2 and MODIS-derived GPP in $10° \times 10°$ bins centered on 35°N, 45°N, 55°N, and 65°N for 36 longitude bins from 180°W to 180°E of equal size. We examine the month of July where we expect the highest GPP values and compare CO_2 concentrations from AIRS to the MODIS-derived GPP for each bin (except for those regions that failed quality control, primarily over oceans). Results give a correlation coefficient of −0.16, −0.80, −0.45 and −0.16 for 35°N, 45°N, 55°N, and 65°N, respectively, between the two data sets. Figure 11 shows the case of highest correlation at 45°N with each longitude region represented by a different color. The high correlation in this zone indicates a significant influence of the surface on midtropospheric CO_2 when and where the GPP is high.

The above correlation analysis was inspired by a time series of AIRS CO_2 and MODIS EVI Level 3 products shown in Video 1. In this video, we present the 12 AIRS CO_2 monthly climatologic means in a loop synchronized with a time series of MODIS normalized difference vegetation index, similar to EVI and GPP, averaged over the period 2003–2006. Use of the climatologic means removes the annual increase due to anthropogenic sources, leaving the seasonal cycle variability due to atmospheric circulation and the interaction with the surface biosphere. The AIRS data are spatially and temporally smoothed using a Fixed Rank Kriging algorithm to improve the horizontal sampling of the AIRS data and match the MODIS time resolution. We see the annual buildup of CO_2 in the NH with a maximum around May. The maximum in the vegetation cycle follows the maximum in CO_2, occurring in late summer. Following the

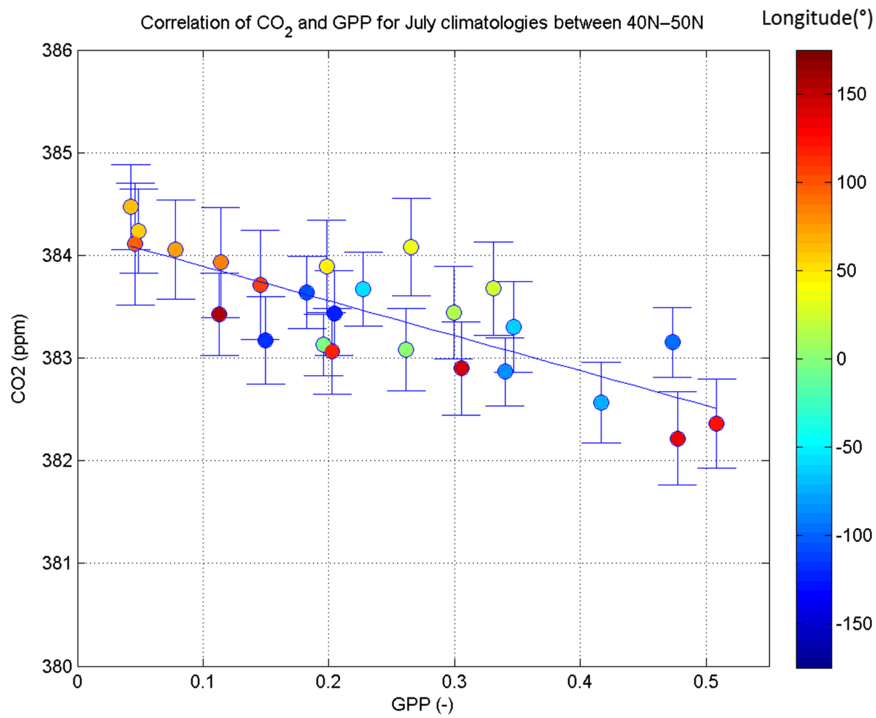

Fig. 11 Correlation of AIRS midtropospheric CO_2 and MODIS-derived GPP for the month of July, for 10° × 10° bins centered at 45°N latitude from 180°W to 180°E longitude. High correlation (−0.80) indicates a strong influence of the boreal forests on the seasonal drawdown of midtropospheric CO_2.

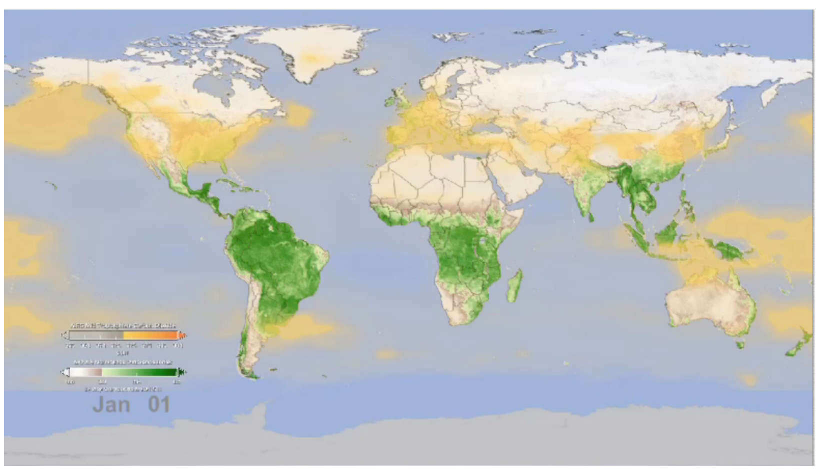

Video 1 Interpolated AIRS midtropospheric CO_2 (orange) overlaid with MODIS Normalized Difference Vegetation Index (NDVI) (green). The time series highlights the regional correlation between the surface and midtroposphere, particularly in the boreal forest of Asia and North America (Video 1, MOV, 10.1 MB) [URL: http://dx.doi.org/10.1117/1.JRS.8.084984.1].

peak in the vegetation, the drawdown of atmospheric CO_2 due to photosynthesis is apparent, particularly over the boreal forest areas in the NH. The video was produced by the NASA science visualization studio and is available on their website at http://svs.gsfc.nasa.gov/vis/a000000/a003900/a003947/index.html.

5 Summary and Conclusions

The AIRS instrument provides valuable midtropospheric CO_2 measurements that cover the time frame from 2003 to the present. Prior efforts have shown that the AIRS CO_2 data are consistent with aircraft measurements with a bias of +0.43 ppm and an RMS deviation of 1.2 ppm, and with TCCON with a bias of −1.8 ppm and a relative accuracy of better than 1 ppm. These levels of precision and accuracy are validated in the mid to northern latitudes and are sufficient to observe the influence of atmospheric circulation and large-scale CO_2 sources and sinks in these regions.

AIRS CO_2 data have enabled observation of small changes in midtropospheric CO_2 associated with vertical transport due to seasonal and interannual oscillations (e.g., MJO and ENSO) as well as general features of the global circulation, including a persistent depression in CO_2 concentrations in the South Atlantic due to a downwelling branch of the Walker circulation.[42] In this paper, we show the impact of surface sources and sinks on the midtropospheric CO_2 levels including generally higher CO_2 levels in the NH extratropics and a high seasonal component in the NH subpolar region. We also show a dampening of the seasonal amplitude from the surface to the midtroposphere in the NH, and an increase in the seasonal amplitude as we move poleward from the equator. There exists a distinct phase lag of about 1–4 months between the surface and the midtroposphere in the NH mid latitudes that has been seen to a lesser extent in aircraft observations and models. Further investigation is needed to better understand the differences. In the SH, we see the phase of the seasonal cycle of midtropospheric CO_2 from AIRS lead that of the surface with higher amplitude, both due to interhemispheric transport. Lastly, good correlation is seen between surface MODIS-derived GPP and AIRS midtropospheric CO_2 where the seasonality of GPP is greatest (NH subpolar). High uncertainty in the AIRS data in the polar regions and a lack of correlative data in the polar midtroposphere leads to inconclusive results in these regions. These results identify a clear influence of surface sources and sinks on CO_2 in the midtroposphere in addition to global circulation patterns, weather, and climate variability.

The synergy of AIRS midtropospheric measurements with the NASA OCO-2 mission is expected to be high. OCO-2 will measure a total column XCO_2 that, when used in conjunction with the AIRS midtropospheric CO_2 data, will improve the information content near the surface compared to OCO-2 alone. In addition, AIRS measures upwelling thermal infrared radiances, allowing measurements and retrievals in the high-northern latitudes at times of year that are unavailable to OCO-2 due to low sun angle. Finally, AIRS CO_2 data can be acquired in modestly cloudy areas such as the tropics, where OCO-2 will have difficulty. Retrieval and data assimilation studies are underway at JPL to realize these benefits in the coming years.

Future work will include incorporating the AIRS Version 6 CO_2 data product into the comparisons. This product is built on an improved AIRS Version 6 temperature and water vapor product that has significantly higher yield and accuracy compared with Version 5, particularly in the polar regions. Version 6 accommodates the loss of AMSU channel 5 that significantly impacted the yield of the AIRS Version 5 CO_2 retrievals after 2010, and will enable the analysis to consider the full AIRS mission data set. Alternate sources of MODIS-derived GPP and chlorophyll fluorescence will also be included in the comparisons.

Acknowledgments

The research described in this paper was carried out at the Jet Propulsion Laboratory, California Institute of Technology, under a contract with the National Aeronautics and Space Administration. The authors would like to acknowledge the late Dr. Moustafa T. Chahine in providing ideas and inspiration for this work.

References

1. IPCC 2013, “Climate Change 2013,” *The Physical Science Basis, Contribution of Working Group 1 to the Fifth Assessment Report of the Intergovernmental Panel on Climate Change*, T. F. Stocker et al., Eds., p. 1535, Cambridge University Press, Cambridge, United Kingdom and New York, NY (2013).
2. C. D. Keeling et al., “Increased activity of northern vegetation inferred from CO2 measurements,” *Nature* **382**, 146–149 (1996).
3. T. J. Conway et al., “Evidence for interannual variability of the carbon cycle for the national oceanic and atmospheric administration/climate monitoring diagnostics laboratory global air sampling network,” *J. Geophys. Res.* **99**(D11), 22831–22855 (1994).

4. D. Wunch et al., "The total carbon column observing network," *Phil. Trans. R. Soc.* **369** (2011), http://dx.doi.org/10.1098/rsta.2010.0240.
5. A. Karion et al., "AirCore: an innovative atmospheric sampling system," *J. Atmos. Oceanic Technol.* **27**, 1839–1853 (2010), http://dx.doi.org/10.1175/2010JTECHA1448.1.
6. Y. Sawa, T. Machida, and H. Matsueda, "Aircraft observation of the seasonal variation in the transport of CO2 in the upper atmosphere," *J. Geophys. Res.* **117**, D05305 (2012), http://dx.doi.org/10.1029/2011JD016933.
7. T. J. Shuck et al., "Greenhouse gas analysis of air samples collected onboard the CARIBIC passenger aircraft," *Atmos. Meas. Tech.* **2**, 449–464 (2009), http://dx.doi.org/10.5194/amt-2-449-2009.
8. S. C. Wofsy et al., "HIAPER pole-to-pole observations (HIPPO): fine-grained, global-scale measurements of climatically important atmospheric gases and aerosols," *Phil. Trans. R. Soc.* **369** (2011), http://dx.doi.org/10.1098/rsta.2010.0313.
9. O. Schneising et al., "Atmospheric greenhouse gases retrieved from SCIAMACHY: comparison to ground-based FTS measurements and model results," *Atmos. Chem. Phys.* **12**, 1527–1540, (2012), http://dx.doi.org/10.5194/acp-12-1527-2012.
10. T. Yakota et al., "Global concentrations of CO2 and CH4 retrieved from GOSAT: first preliminary results," *SOLA* **5**, 160–163, (2009), http://dx.doi.org/10.2151/sola.2009-041.
11. D. Crisp et al., "The orbiting carbon observatory (OCO) mission," *Adv. Space Res.* **34**(4), 700–709 (2004).
12. M. T. Chahine et al., "Satellite remote sounding of mid-tropospheric CO2," *Geophys. Res. Lett.* **35**(17), L17807 (2008), http://dx.doi.org/10.1029/2008GL035022.
13. C. Crevoisier et al., "First year of upper tropospheric integrated content of CO2 from IASI hyperspectral infrared observations," *Atmos. Chem. Phys.* **9**, 4797–4810 (2009), http://dx.doi.org/10.5194/acp-9-4797-2009.
14. S. S. Kulawik et al., "Characterization of tropospheric emission spectrometer (TES) CO2 for carbon cycle science," *Atmos. Chem. Phys.* **10**, 5601–5623 (2010), http://dx.doi.org/10.5194/acp-10-5601-2010.
15. R. Miao et al., "Multi-year comparison of carbon dioxide from satellite data with ground-based FTS measurements (2003–2011)," *Remote Sensing* **5**(7), 3431–3456 (2013), http://dx.doi.org/10.3390/rs5073431, http://www.mdpi.com/2072-4292/5/7/3431.
16. R.-L. Shia et al., "CO2 in the upper troposphere: influence of stratosphere-troposphere exchange," *Geophys. Res. Lett.* **33**, L14814 (2006), http://dx.doi.org/10.1029/2006GL026141.
17. Li. King-Fai et al., "Mid-tropospheric CO2 variability driven by the Madden–Julian oscillation," *PNAS* **107**(45), 19171–19175 (2010), http://dx.doi.org/10.1073/pnas.1008222107.
18. X. Jiang et al., "Interannual variability of mid-tropospheric CO2 from atmospheric infrared sounder," *Geophys. Res. Lett.* **37**, L13801 (2010), http://dx.doi.org/10.1029/2010GL042823.
19. X. Jiang et al., "Influence of El Nino on Midtropospheric CO2 from atmospheric infrared sounder and model," *J. Atmos. Sci.* **70**(1), 223–230 (2013), http://dx.doi.org/10.1175/JAS-D-11-0282.1.
20. L. Feng et al., "Evaluating a 3-D transport model of atmospheric CO2 using ground-based, aircraft and space-borne data," *Atmos. Chem. Phys.* **11**, 2789–2803 (2011), http://dx.doi.org/10.5194/acp-11-2789-2011.
21. X. Jiang et al., "Influence of stratospheric sudden warming on AIRS midtropospheric CO2," *J. Atmos. Sci.* **70**, 2566–2573 (2013), http://dx.doi.org/10.1175/JAS-D-13-064.1.
22. F. V. Cochran, N. A. Brunsell, and D. B. Mechem, "Comparing surface and mid-tropospheric CO2 concentrations from Central US grasslands," *Entropy* **15**(2), 606–623 (2013), http://dx.doi.org/10.3390/e15020606, http://www.mdpi.com/1099-4300/15/2/606/pdf.
23. Y. Hou et al., "Variations of greenhouse gas carbon dioxide concentration over the Chinese mainland based on satellite and background measurements," *Disaster Advances* **5**(4), 1773–1779 (2012).
24. R. J. Engelen, S. Serrar, and F. Chevallier, "Four-dimensional data assimilation of atmospheric CO2 using AIRS observations," *J. Geophys. Res.* **114**, D03303 (2009), http://dx.doi.org/10.1029/2008JD010739.

25. J. Liu et al., “Simultaneous assimilation of AIRS XCO2 and meteorological observations in a carbon climate model with an ensemble Kalman filter,” *J. Geophys. Res.* **117**, D05309 (2012), http://dx.doi.org/10.1029/2011JD016642.
26. H. H. Aumann et al., “AIRS/AMSU/HSB on the Aqua mission: design, science objectives, data products, and processing systems,” *IEEE Trans. Geosci. Remote Sens.* **41**(2), 253–264 (2003), http://dx.doi.org/10.1109/TGRS.2002.808356.
27. T. S. Pagano, M. T. Chahine, and E. T. Olsen, “Seven years of observations of mid-tropospheric CO2 from the atmospheric infrared sounder,” *Acta Astronautica* **69**(7–8), 35–359 (2011), http://dx.doi.org/10.1016/j.actaastro.2011.05.016.
28. J. Susskind et al., “Improved temperature sounding and quality control methodology using AIRS/AMSU data: the AIRS science team version-5 retrieval algorithm,” *IEEE Trans. Geosci. Remote Sens.* **49**, 883–907 (2011), http://dx.doi.org/10.1109/TGRS.2010.2070508.
29. M. T. Chahine et al., “On the determination of atmospheric minor gases by the method of vanishing partial derivatives with application to CO2,” *Geophys. Res. Lett.* **32**(22), L22803 (2005), http://dx.doi.org/10.1029/2005GL024165.
30. T. Machida et al., “Worldwide measurements of atmospheric CO2 and other trace gas species using commercial airlines,” *J. Atmos. Ocean. Tech.* **25**, 1744–1754 (2008), http://dx.doi.org/10.1175/2008JTECHA1082.1.
31. J. Susskind, J. M. Blaisdell, and L. Iredell, “Improved methodology for surface and atmospheric soundings, error estimates, and quality control procedures: the AIRS science team version-6 retrieval algorithm,” *J. Appl. Remote Sens.* **8**(1), 084994 (2014).
32. K. Miyazaki et al., “Formation mechanisms of latitudinal CO2 gradients in the upper troposphere over the subtropics and tropics,” *J. Geophys. Res.* **114**, D03306 (2009), http://dx.doi.org/10.1029/2008JD010545.
33. C. Wang, “Atlantic climate variability and its associated atmospheric circulation cells,” *J. Climate* **15**, 1516–1536 (2002), http://dx.doi.org/10.1175/1520-0442(2002)015<1516:ACVAIA>2.0.CO;2.
34. J. Susskind et al., “Improved temperature sounding and quality control methodology using AIRS/AMSU data: the AIRS science team version 5 retrieval algorithm,” *IEEE Trans. Geosci. Remote Sens.* **49**(3), 883–907 (2011), http://dx.doi.org/10.1109/TGRS.2010.2070508.
35. T. J. Conway, P.M. Lang, and K.A. Masarie, “Atmospheric carbon dioxide dry air mole fractions from the NOAA ESRL carbon cycle cooperative global air sampling network,” 1968–2010, Version: 2011-10-14, Path: ftp://ftp.cmdl.noaa.gov/ccg/co2/flask/event/ (2011),
36. C. Beer et al., “Terrestrial gross carbon dioxide uptake: dlobal distribution and covariation with climate,” *Science* **329**, 834–838, (2010), http://dx.doi.org/10.1126/science.1184984.
37. A. Huente et al., “Overview of the radiometric and biophysical performance of the MODIS vegetation indices,” *Remote Sens. Environ.* **83**, 195–213 (2002), http://dx.doi.org/10.1016/S0034-4257(02)00096-2.
38. Z. Wan, “New refinements and validation of the MODIS Land-Surface temperature/emissivity products,” *Remote Sens. Environ.* **112**, 59–74 (2008), http://dx.doi.org/10.1016/j.rse.2006.06.026.
39. A. Sims et al., “A new model of gross primary productivity for North American ecosystems based soley on the enhanced vegetation and land surface temperature from MODIS,” *Remote Sens. Environ.* **112**, 1633–1646 (2008), http://dx.doi.org/10.1016/j.rse.2007.08.004.
40. A. Ruzmaikin, H. H. Aumann, and T. S. Pagano, “Patterns of CO2 variability from global satellite data,” *J. Climate* **25**, 6383–6393 (2012), http://dx.doi.org/10.1175/JCLI-D-11-00223.1.
41. X. Jiang et al., “CO2 semiannual oscillation in the middle troposphere and at the surface,” *Global Biogeochem. Cycles* **26**, GB3006 (2012), http://dx.doi.org/10.1029/2011GB004118.
42. X. Jiang et al., “Modulation of mid-tropospheric CO2 by the South Atlantic circulation,” Submitted to GRL (2014).

Thomas S. Pagano is the project manager for the AIRS/AMSU/HSB Suite of instruments on the EOS Aqua Spacecraft. He was the lead engineer responsible for the calibration of the AIRS instrument in orbit. Prior to joining JPL in 1997, he was the chief systems engineer on the MODIS instrument development program at Raytheon SBRS since 1985. He received a BS degree in physics from University of California Santa Barbara, California and an MS degree in physics from Montana State University, Montana. He holds two US patents and is the author of numerous papers on space remote sensing systems.

Edward T. Olsen works at the Jet Propulsion Laboratory, Pasadena, California and leads the AIRS CO_2 retrieval and validation task. He is responsible for the AIRS user services and supports the AIRS applications development task. He has a BS in Physics from MIT, an MS in Physics from Caltech and a Ph.D. in Astronomy from the University of Michigan.

Hai Nguyen graduated in 2009 from University of California, Los Angeles, receiving a doctorate degree in statistics. He then joined the Jet Propulsion Laboratory as a post-doc and as a full-time employee in 2011. Hai's areas of interest include spatial statistics, machine learning, and optimal estimation. His current projects at JPL include developing data fusion methodology for combining data from different remote sensing instruments and error characterization for the ACOS project.

Alexander Ruzmaikin is a principal scientist at the Jet Propulsion Laboratory, California Institute of Technology. He received his masters degree in engineering and PhD in space science from Moscow Phystech, which was founded and led by Nobel Laureates in Physics P. Kapitza and L. Landau. Currently he is a member of the AIRS team involved in data verification and climate studies.

Xun Jiang graduated with a BS in atmospheric science from Nanjing University of Information Science & Technology in 1998, an MS in meteorology from Peking University in 2001, and a PhD in environmental science and engineering from California Institute of Technology in 2006. Now, she is an associate professor of atmospheric sciences at the University of Houston.

Lori Perkins is a computer engineer at NASA Goddard Space Flight Center. She has written ground systems software for EUVE, Sampex, Swift, Trace, Wind, Polar, ACES, XTE, SOHO, TRMM, LandSat 5, MAP and IMAGE projects. Now, she specializes in data visualization from remote sources. Data visualizers combine different information collected from different sources to highlight the diverse work of NASA's scientific community. She focuses on creating informative visualizations that accurately represent the underlying information.